Int. J. Electrochem. Sci., 15 **(2020)** 4660 – 4670, doi: 10.20964/2020.05.81

International Journal of
ELECTROCHEMICAL
SCIENCE
www.electrochemsci.org

Short Communication

Electrochemical Behavior of Carbon Fiber - Coupled Steel in Concrete Environment

Chun Bai[1,2,3,4], Shuxian Liu[1], Fenghai Ma[2], Shasha Lu[1,], Junmei Wang[3,4], Shaodong Liu[1]*

[1] College of Civil Engineering, Liaoning Technical University, Fuxin, Liaoning, 123000, P.R. China
[2] College of Architecture and Civil Engineering Dalian University, Dalian, Liaoning, 116622, P.R. China
[3] College of Civil Engineering, Xuchang University, Xuchang, Henan, 461000, P.R. China
[4] College of Architecture and Civil Engineering, Shangqiu University, Shangqiu Henan, 476000, P.R. China
[*]E-mail: bianqiao82536967@163.com

Received: 1 January 2019 / *Accepted:* 17 February 2020 / *Published:* 10 April 2020

As a new structural building material, carbon fiber-reinforced concrete has very good flexural strength, wear resistance and impermeability. However, because carbon fiber is a good conductor, the durability of reinforced concrete structures may be affected if it comes into contact with steel bars in the concrete, thus allowing the formation of a galvanic couple. In this paper, electrochemical tests and corrosion weightlessness experiments were carried out in a pore fluid of concrete with a pH of 12.5. The results showed that when carbon fiber was coupled with carbon steel, the double layer capacitance (C_{dl}) increased and the charge transfer resistance (R_{ct}) decreased. The thickness of the passivation film decreased, and the protective performance of the passivation film on the carbon steel decreased. Moreover, the corrosion potential of the carbon steel increased, the corrosion current density increased, and the corrosion rate of the carbon steel increased. An XPS analysis confirmed the results of the electrochemical experiments. After carbon fiber coupling, the ratio of Fe^{3+}/Fe^{2+} on the surface of the carbon steel decreased, and the stability of the passive film on the surface of the carbon steel decreased. Although coupling with carbon fiber had a negative effect on the passivation of the carbon steel, the surface of the carbon steel could still maintain good passivation in a chloride-free simulated pore fluid environment.

Keywords: Concrete pore fluid, Cement mortar, Reinforcement, Carbon fiber, pH value, Electrochemical analysis

1. INTRODUCTION

Reinforced concrete refers to a composite structural building material composed of steel and concrete. Among them, concrete is a kind of artificial stone material that is composed of cementitious

material, water, and coarse and fine aggregate that are all mixed in a proper proportion and then hardened for a period of time [1–4]. Concrete structures are durable and have a high compressive strength. However, they also have some disadvantages, such as an obvious deficiency in tensile strength. Generally, its tensile strength is only one-tenth of its compressive strength. Under a large bending stress, the concrete structure easily cracks and then fails [5–8]. The concrete structure is not resistant to bending stress, which limits its application to a large extent. At present, the corrosion and protection measures of reinforced concrete structures have become a very concerning and focused research problem in international related fields [9–15]. Through a case study of steel corrosion in different concrete, reasonable corrosion protection measures are used to extend the service life of reinforced concrete [16–19]. The application of fiber composite materials in the field of civil engineering began in the 1970s. In the late 20th century, the mass production of engineering fiber was realized. The price of fiber in the international material market has been greatly reduced, and the strengthening of concrete structures with fiber-reinforced composite materials has become an economic and feasible method, which has gradually attracted the attention of experts in the construction field. Among them, the reinforcement of concrete structures with carbon fiber composites has begun to gradually replace the traditional method [20–22].

As a new composite material, carbon fiber reinforced concrete has not only excellent physical and chemical properties but also better flexural strength, compressive strength, wear-resistance and impermeability compared to that of traditional concrete. In addition, due to the good conductivity of carbon fiber, the concrete structure after adding carbon fiber can also meet some special requirements, such as meeting the requirements of concrete stress monitoring, shielding electromagnetic interference and reducing the driving voltage of concrete during cathodic protection [23–26]. However, carbon fiber has a large specific surface area, which may affect the porosity and permeability of concrete after being mixed with concrete; furthermore, it may affect the corrosion of steel bars in concrete, and thus the durability of concrete. The research of Hou et al. [27] shows that adding 0.5% (mass fraction of cement) carbon fiber can reduce the volume resistivity of concrete, thus reducing the corrosion resistance of steel bars in concrete, especially in corrosive environments with high concentrations of chloride ions. Garces et al. [28] found that adding a certain proportion of carbon fiber into cement will slow down the corrosion of steel bars, and the corrosion degree of steel bars will decrease with an increase in the amount of carbon fiber. Therefore, there is no clear conclusion about the influence of carbon fiber on the corrosion of steel bars in carbon fiber reinforced concrete structures. Therefore, there is no clear conclusion about the influence of carbon fiber on the corrosion of steel bars in carbon fiber-reinforced concrete structures. In addition, carbon fiber is a kind of conductive material and has a positive potential compared with steel bars [29–34]. If it comes into contact with a steel bar in the concrete structure, it will produce a galvanic effect.

The methods of detecting the corrosion degree of steel bars in concrete can be divided into physical methods and electrochemical methods. Physical methods include the ray method, resistance method, acoustic emission method, impact echo method, eddy current method, magnetic field method and ultrasonic method [35–39]. The principle of using physical detection means that the physical properties of steel bars have changed before and after corrosion, such as shape, size, electrical performance, thermal performance and other physical properties. Therefore, the corrosion and degree can be determined by detecting these physical indicators during the service period of steel bars in

concrete [40–42]. In essence, the occurrence of steel corrosion in concrete is actually the result of a series of complex electrochemical reaction processes, so the use of electrochemical field test methods can more accurately describe the corrosion process and degree of steel in concrete. Electrochemical methods are used in the field of corrosion detection, and different monitoring methods are derived according to different needs [43–45]. Generally, corrosion detection in engineering practice requires that the impact and disturbance of the detection method on the material be as small as possible, so it is generally necessary to select an in situ nondestructive testing method. In this paper, the influence of carbon fibers on the corrosion behavior of steel bars in a concrete environment is studied systematically, and the influence of the pH value on the system is studied deeply.

2. EXPERIMENTAL

Once the carbon fiber and steel bar are in contact with the aqueous solution at the same time, the potential difference between the two naturally forms an electric pair, local corrosion occurs when steel bars act as anodes. Therefore, the study of the corrosion of the carbon fiber coupled to steel in concrete environment is essential. The carbon fiber used in the experiment is CCF303K carbon fiber. The carbon steel sample used in the electrochemical experiment is Q235 carbon steel reinforcement, which is processed into a sample with a diameter of 1.0 cm and a length of 1 cm. The front side is used as the working surface, the back side is welded to a copper wire lead, and the side and back side are sealed with epoxy resin; thus, an electrochemical test electrode is made. Before the test, the steel sample is polished with sandpaper, washed with deionized water, wiped with acetone and alcohol, and dried with hot air before use. Before the test, the working surface is sealed with epoxy resin, leaving a working surface of 0.4 cm^2.

Preparation of the carbon fiber sample: A bunch of carbon fiber is wound around a PVC plastic sheet. The back of the PVC sheet is covered with epoxy resin to make the carbon fiber on the front side contact the copper wire. The length of the carbon fiber on the front of the PVC plastic sheet is 5 cm. A carbon fiber coupled carbon steel specimen is made by connecting the outer end of the carbon fiber specimen and the reinforcement specimen with an electric wire.

Concrete pore medium preparation: A saturated calcium hydroxide solution serves as the concrete pore medium solution. The pH value is approximately 10. The mass fraction of NaCl in the concrete pore medium is 1.0%. The concentration of sodium molybdate is 0.5 g/L. All reagents are analytically pure and are provided by Shanghai Aladdin Bio-Chem Technology Co., LTD. Distilled water is used for dissolution.

Electrochemical analysis: The polarization curve is measured by a CS350 electrochemical system. The initial potential is the open circuit potential, and the scanning rate is 0.5 mV/s. The working electrode is a carbon steel sample, carbon fiber sample or carbon steel sample coupled with a carbon fiber sample. The reference electrode is a saturated calomel electrode, and the auxiliary electrode is a platinum electrode. A CS350 electrochemical test system is also used for the galvanic current test. The carbon steel sample is connected with WE2, the carbon fiber sample is connected with WE1, and a saturated calomel electrode is used as the reference electrode for current and potential monitoring. The

polarization parameters, such as corrosion current density, corrosion potential, and breakdown potential, are analyzed with software attached to the test instrument. EIS measurements are performed at the open-circuit potential. The frequency range is from 100 kHz to 0.01 Hz. The amplitude of the signal is 5 mV.

3. RESULTS AND DISCUSSION

The open circuit potential of the carbon steel sample, carbon fiber coupled to steel and carbon fiber sample in a pore fluid with a pH of 10 are monitored. The test time is 2 h, and the results are shown in Figure 1A. In the figure, the corrosion potential of the carbon steel sample first increases rapidly, reaches its highest potential value of - 120 mV in 0.25 h, and then decreases slowly; after 2 h, it is approximately - 170 mV. It can be seen that the potential of the carbon steel sample can basically be stable after soaking in the pore solution at pH 10 for 2 h. Therefore, before the subsequent polarization curve and impedance test, the carbon steel sample is prepassivated in the pore solution for 2 h. In Figure 1A, the corrosion potential of the carbon fiber sample basically changes little with the extension of immersion time. The corrosion potential of the carbon fiber coupled to steel increase slightly with immersion time and stabilize at -104 mV after 1 h. The corrosion potential of carbon steel with carbon fiber coupling is between that of carbon fiber and carbon steel, which is slightly negative than that of carbon fiber [46–48]. The results show that carbon steel has an anodic polarization after coupling with carbon fiber.

The anodic polarization curve of the carbon steel sample is tested after 2 h of prepassivation, and the results are shown in Figure 1B. It can be seen that carbon steel is in a good passivation state in a potential range of 0 mV-600 mV. The passivation potential of carbon steel increases, and the passivation area narrows after coupling with carbon fiber. The increase in corrosion current density is by approximately one order of magnitude, which shows that the passivation ability of carbon steel decreases and the corrosion rate increases after coupling with carbon fiber.

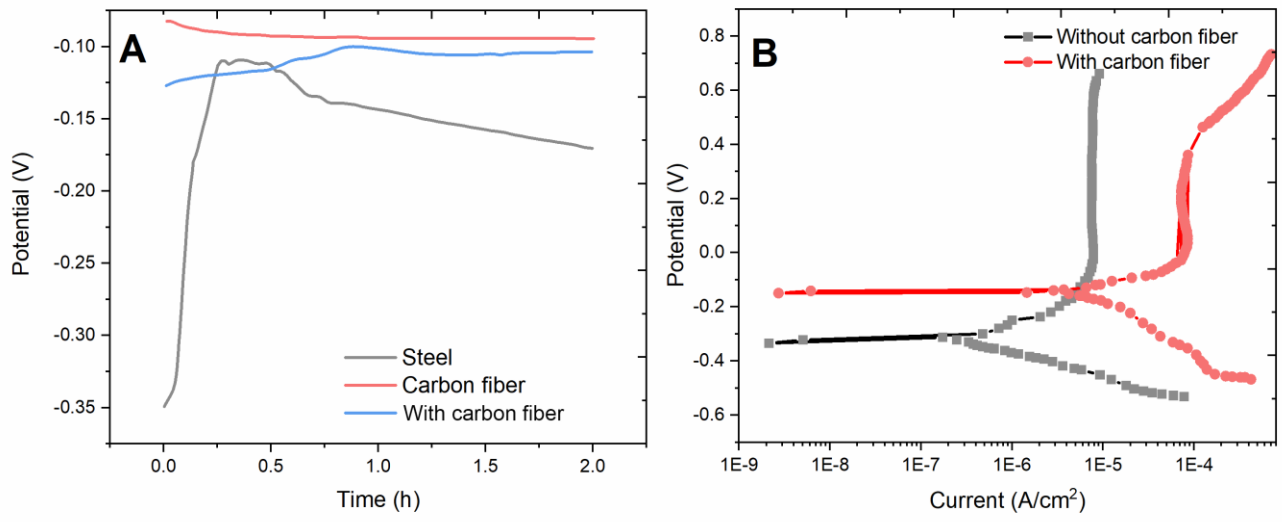

Figure 1. (A) Open circuit potential – time curves of steel, carbon fiber sample and carbon fiber coupled to steel in the pH 10 pore solution. (B) Polarization curves of the steel and carbon fiber coupled to steel in the pH 10 pore solution.

The EIS test provides potential, impedance and phase angle data for the chosen frequency spectrum. These data can be plotted in different formats to better understand the corrosion state of the system, coating saturation and resistivity of the concrete [49–52]. A Bode plot is plotted with the modulus of impedance and the phase angle as a function of the frequency of the alternating current. On the other hand, the Nyquist plot presents real and imaginary components of the complex impedance response [53–55]. After the prepassivation treatment of the carbon steel sample, an impedance test is carried out, and the results are shown in Figure 2A. The impedance spectrum of carbon steel in the simulated pore fluid of concrete has an obvious capacitive arc in the middle and low frequency, which reflects the electrochemical characteristics of the carbon steel surface. The radius of the capacitive arc is smaller than that of carbon steel. Figure 2B shows that the impedance value of carbon steel coupled with carbon fiber at 0.01 Hz is 3×10^3 Ω·cm^2. The $|Z|_{0.01Hz}$ of carbon steel without the carbon fiber coupling is 8×10^5 Ω·cm^2. Therefore, the resistance of carbon steel will be reduced after coupling with carbon fiber. In the impedance phase angle diagram (Figure 2C), a new peak appears in a frequency range of 10-1000 Hz, which indicates that a time constant is added to the impedance diagram after coupling with carbon fiber. The reason for the decrease in the low-frequency impedance value of carbon steel after coupling with carbon fiber is that the resistance value of the carbon fiber sample decreases after coupling, and it may also come from the contribution of the decrease in the surface impedance value of carbon steel [56–58]. To obtain the information of the carbon steel surface, equivalent circuit fitting of the impedance spectrum is carried out. Table 1 shows the coupling of the carbon fiber on the fitted parameters of the EIS diagrams for reinforcement. Upon coupling the carbon fiber to the steel, both R_c and R_{ct} increase significantly. The film resistance of the corrosion products and the charge transfer resistance of the electrochemical reaction are markedly enhanced. In general, the passivation film and corrosion product films on the metal surface possess semiconductor properties. Based on the Mott–Schottky theory, the film is an n-type semiconductor when the slope of the Mott–Schottky curve is positive and a p-type semiconductor when the slope is negative [59–61].

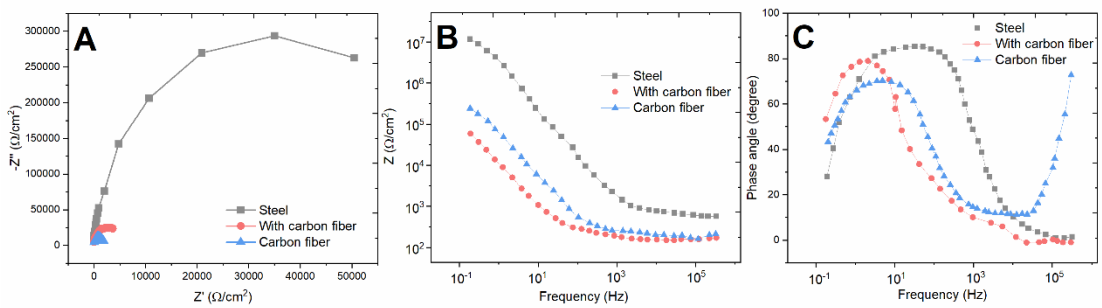

Figure 2. (A) Nyquist plots, (B-C) Bode plots of the steel and steel samples with carbon fibers in the pH 10 pore solution.

The prepared carbon steel sample and carbon steel sample coupled with carbon fiber are prepassivated in the pore liquid with a pH of 10 for 2 h. After treatment, the surface is dried with alcohol for XPS testing. The test results are shown in Figure 3. Figure 3A shows the total spectrum, and 3b

shows the narrow scanning spectrum and split peak fitting of Fe. As shown in Figure 3a, the surface of carbon steel after prepassivation in the pH 10 pore solution contains four elements: C, Ca, O and Fe. Since C is an external standard element, its content is greatly affected by pollutants. The content of Ca on the surface of carbon steel is 2.81%, which is mainly from the deposition of $Ca(OH)_2$ and $CaCO_3$ on the surface of carbon steel.

Table 1. EIS parameters of the steel and steel samples with carbon fibers in the pH 10 pore solution.

Sample	Rs (Ω/cm^2)	n_c	Rc (Ω/cm^2)	n_{dl}	Rct ($k\Omega/cm^2$)
Steel	5.5	11.2	0.23	0.282	0.31
With carbon fiber	6.2	2.25	18.51	0.505	80.07
Carbon fiber	5.1	3.51	9.66	0.407	62.25

O mainly exists with the Fe, Ca and impure water [62–65]. The Fe on the surface of the carbon steel undergoes a narrow scan, and the results are shown in Figure 3B. The passive film of carbon steel in the simulated pore fluid may contain FeOOH, Fe_2O_3, FeO, Fe_3O_4, Fe_3C and Fe. Fe^{3+} is found in FeOOH, Fe_2O_3 and Fe_3O_4, and its characteristic peak is 710.8 eV. Fe^{2+} is in FeO and Fe3O4, and its characteristic peaks are 709.6 eV and 714 eV. The characteristic peak of Fe in cementite Fe_3C is 707.3 eV and that of Fe is 706.6 eV. According to the fitting calculation, Fe^{3+} accounts for 61.7% of the total Fe content, Fe^{2+} accounts for 16.9% of the total Fe content, Fe accounts for 11% of the total Fe content in Fe_3C, and Fe accounts for 8.9% of the total Fe content. It can be seen from the narrow spectrum of Fe that the passivation film formed on the surface of carbon steel is mainly composed of Fe^{3+}, with the presence of small amounts of Fe^{2+}, Fe_3C and Fe. Based on the above analysis, the surface corrosion products of casing steel can be speculated to be mainly composed of $FeCO_3$, Fe_3O_4 and a small amount of $Fe(OH)_2$. $FeCl_2$ is an intermediate product that forms during the catalytic corrosion of steel [66–70].

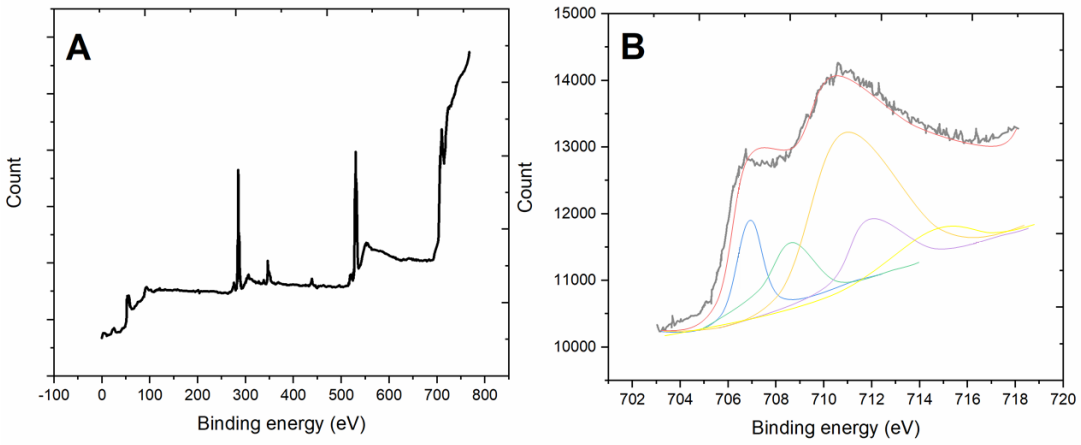

Figure 3. (A) XPS survey and (B) Fe 2p3/2 scan for the steel in the pH 10 concrete pore solution.

Figure 4 is the XPS scanning spectrum of the prepassivated carbon steel sample coupled with carbon fiber; Figure 4A is the total spectrum and 4B is the narrow scanning spectrum and peak fitting of Fe. The results show that the content of $Ca(OH)_2$ and CaO_3 on the surface of carbon steel decreases after coupling with carbon fiber; that is, the content of $Ca(OH)_2$ and CaO_3 on the surface of the carbon steel decreases after coupling with carbon fiber. The results show that Fe^{3+} is 62.6%, Fe^{2+} is 21.7%, Fe_3C is 5.1%, and Fe is 8.2%. It can be seen from the narrow spectrum of Fe that the content of Fe^{2+} on the surface of the carbon steel increases after coupling with carbon fiber. The content ratio of Fe^{3+} and Fe^{2+} is used to measure the protective performance of the passive film. The higher the ratio of Fe^{3+}/Fe^{2+} is, the higher the FeOOH and Fe_2O_3 content in the film, and the better the stability of the film. In contrast, the lower the ratio is, the higher the content of FeO and Fe_3O_4 in the film, and the film is more unstable; in other words, the protection performance of the film is worse. Comparing the Fe^{3+}/Fe^{2+} content ratio of the carbon steel film before and after coupling, it is found that the Fe^{3+}/Fe^{2+} ratio decreases after coupling with carbon fiber, which indicates that the Fe^{2+} content of the passive film on the carbon steel surface increases after coupling with carbon fiber, and the protective performance of the passive film on the carbon steel surface decreases.

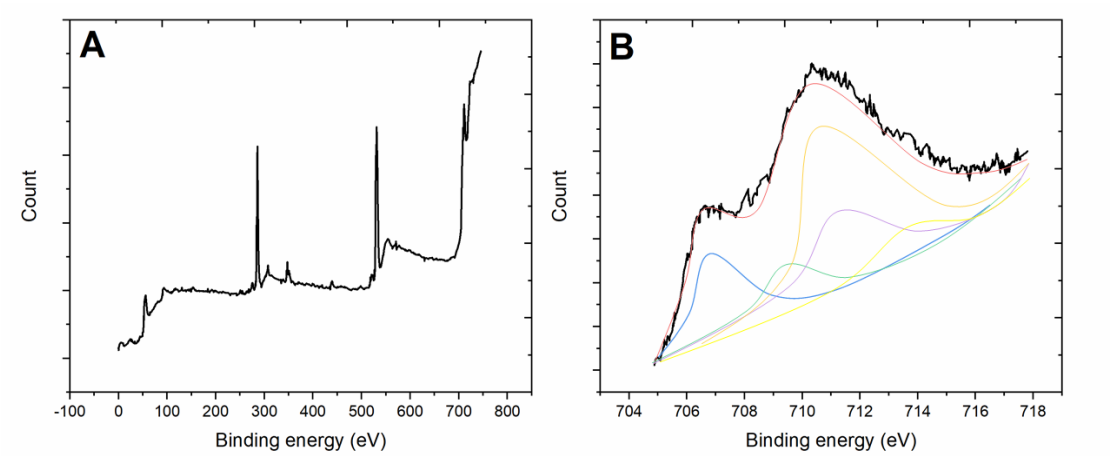

Figure 4. (A) XPS survey and (B) Fe 2p3/2 scan for the carbon fiber coupled to steel in the pH 10 concrete pore solution.

We also studied the effect of coupling different volumes of carbon fiber on the electrochemical behavior of carbon steel by using an anodic polarization curve, an impedance test and an XPS analysis. Figure 5 shows the anodic polarization curve of carbon steel with carbon fibers lengths of 5 cm and 10 cm after the prepassivation treatment. Figure 5 shows that the passivation range of the anodic polarization curve of carbon steel coupled with the 5-cm carbon fiber becomes narrow and the passivation potential increases. The passivation zone of the anodic polarization curve of carbon steel becomes less obvious after the coupling amount is doubled. The current density increases with increasing potential in the anode area. The results show that the passivation ability of the carbon steel surface decreases with an increasing amount of carbon fiber.

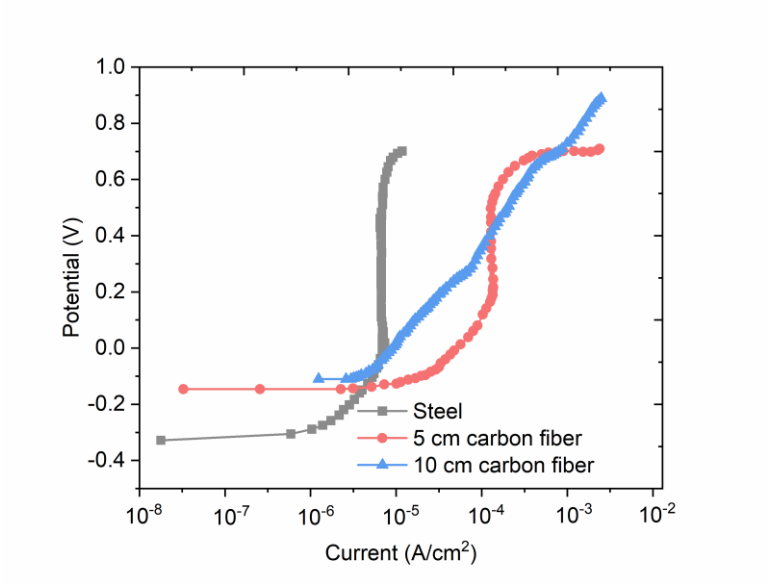

Figure 5. Anodic polarization curves of the carbon steel coupled with 5 cm and 10 cm lengths of carbon fiber in the pH 10 pore solutions.

Figure 6 is the impedance spectrum of the carbon steel coupled with different lengths of carbon fiber. As shown in Figure 6, the spectrum of carbon steel shows little change when coupled with an increasing amount of carbon fiber. After coupling with carbon fiber, the C_{dl} of carbon steel increases by approximately three orders of magnitude, the R_{ct} decreases by approximately five orders of magnitude, the coupling amount of carbon fiber increases by times, and the C_{dl} and R_{ct} decrease slightly; for the C_{dl} and R_{ct}, the change is not large and is still in the same order of magnitude. The changes in impedance C_f and R_f of the carbon steel surface with an alkaline coating are similar to those of C_{dl} and R_{ct}. After the carbon fiber coupling, C_f increases by two orders of magnitude.

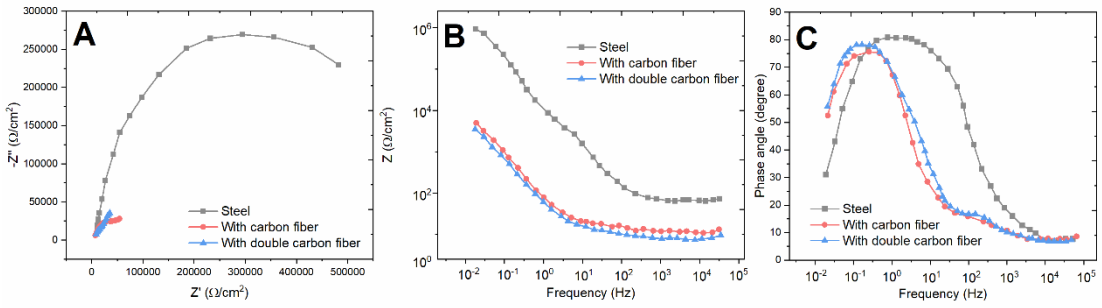

Figure 6. (A) Nyquist plots and (B-C) Bode plots of the steel samples with various amounts of carbon fiber in the pH 10 pore solution.

With the doubling of the coupling amount, C_f increases slightly. R_f decreases by two orders of magnitude after the carbon fiber coupling. With the doubling of the carbon fiber coupling amount, the change is not significant. The impedance values of C_{cf} and R_{cf} on the surface of the carbon fiber remain basically the same. The results of the impedance measurements show that the electrochemical state of

the carbon steel surface is greatly affected by the coupled carbon fiber in the pore solution with a pH of 10; however, the change in C_{dl} and R_{ct} on the surface of the carbon steel is not significant when the coupling amount of carbon fiber is doubled.

An XPS scanning spectrum of the carbon steel sample passivated by coupling with carbon fiber is obtained. According to the peak fitting calculation, Fe^{3+} accounts for 52.5% of the total Fe content, and Fe^{2+} accounts for 21.7% of the total Fe content. At this time, the content ratio of Fe^{3+}/Fe^{2+} is 2.2. In conclusion, with an increase in the amount of carbon fiber, the content of Fe^{3+}/Fe2+ and Fe^{3+} decrease, so the protective performance of the passive film on the surface of the carbon steel decreases with the increase in the amount of carbon fiber.

4. CONCLUSION

We studied the effect of carbon fiber on the corrosion of reinforced concrete in a pH 10 pore solution. It was found that the potential of carbon steel after coupling with carbon fiber shifted positively, and the stable mixed potential was between the carbon fiber and carbon steel. After coupling with carbon fiber, the passivation potential of the carbon steel increased, the corrosion current density increased slightly, and the corrosion rate increased slightly. After coupling with carbon fiber, the thickness of the passivation film on the carbon steel surface decreased, the ratio of Fe^{3+}/Fe^{2+} in the passivation film decreased, and the protective performance of the passivation film on the carbon steel decreased.

ACKNOWLEDGEMENTS
This work was supported by the National Natural Science Foundation of China (51474045); Key Scientific Research Projects of Colleges and Universities in Henan Province (18A560019, 19A560023, 20B560013).

References

1. C. Grengg, F. Mittermayr, N. Ukrainczyk, G. Koraimann, S. Kienesberger, M. Dietzel, *Water Res.*, 134 (2018) 341.
2. C. Jiang, Y.-F. Wu, M.-J. Dai, *Constr. Build. Mater.*, 158 (2018) 1073.
3. Y. Liu, Y. Song, J. Keller, P. Bond, G. Jiang, *Rsc Adv.*, 7 (2017) 30894.
4. C. Grengg, F. Mittermayr, G. Koraimann, F. Konrad, M. Szabó, A. Demeny, M. Dietzel, *Cem. Concr. Res.*, 101 (2017) 93.
5. Y. Song, E. Wightman, Y. Tian, K. Jack, X. Li, H. Zhong, P.L. Bond, Z. Yuan, G. Jiang, *Sci. Total Environ.*, 649 (2019) 739.
6. A. Hendi, A. Behravan, D. Mostofinejad, S.M. Moshtaghi, K. Rezayi, *Constr. Build. Mater.*, 138 (2017) 441.
7. A. Bossio, G.P. Lignola, F. Fabbrocino, T. Monetta, A. Prota, F. Bellucci, G. Manfredi, *Struct. Concr.*, 18 (2017) 104.
8. G. de Vera, M. Miró, E.G. Segovia, P. Poveda, M.Á. Climent, *Appl. Sci.*, 9 (2019) 3061.
9. L. Fu, A. Wang, G. Lai, C.-T. Lin, J. Yu, A. Yu, Z. Liu, K. Xie, W. Su, *Microchim. Acta*, 185 (2018) 87.

10. Y. Zheng, L. Fu, F. Han, A. Wang, W. Cai, J. Yu, J. Yang, F. Peng, *Green Chem. Lett. Rev.*, 8 (2015) 59.
11. L. Fu, A. Wang, G. Lai, W. Su, F. Malherbe, J. Yu, C.-T. Lin, A. Yu, *Talanta*, 180 (2018) 248.
12. L. Fu, Y. Zheng, Q. Ren, A. Wang, B. Deng, *J Ovonic Res*, 11 (2015) 21.
13. L. Fu, W. Cai, A. Wang, Y. Zheng, *Mater. Lett.*, 142 (2015) 201.
14. L. Fu, Z. Fu, *Ceram. Int.*, 41 (2015) 2492–2496.
15. H. Rong, H. Hu, J. Zhang, J. Wang, M. Zhang, G. Qin, Y. Zhang, X. Zhang, *J. Mater. Sci. Technol.*, 35 (2019) 2485.
16. J. Rivera-Corral, G. Fajardo, G. Arliguie, R. Orozco-Cruz, F. Deby, P. Valdez, *Constr. Build. Mater.*, 147 (2017) 815.
17. C. Fu, N. Jin, H. Ye, X. Jin, W. Dai, *Corros. Sci.*, 117 (2017) 11.
18. M.G. Sohail, R. Kahraman, N.A. Alnuaimi, B. Gencturk, W. Alnahhal, M. Dawood, A. Belarbi, *Constr. Build. Mater.*, 232 (2020) 117205.
19. S.V. Fedosov, V.E. Roumyantseva, I.V. Krasilnikov, B.E. Narmania, *Int. J. Comput. Civ. Struct. Eng.*, 13 (2017) 45.
20. W. Nguyen, J.F. Duncan, T.M. Devine, C.P. Ostertag, *Electrochimica Acta*, 271 (2018) 319.
21. H. Mohammadhosseini, M.M. Tahir, A.R.M. Sam, N.H.A.S. Lim, M. Samadi, *J. Clean. Prod.*, 185 (2018) 252.
22. W. Nguyen, J.F. Duncan, G. Jen, C.P. Ostertag, *Corros. Sci.*, 140 (2018) 168.
23. P. Giri, S. Kharkovsky, X. Zhu, S.M. Clark, S. Taheri, B. Samali, *Struct. Health Monit.*, 18 (2019) 172.
24. M. Lu, H. Xiao, M. Liu, X. Li, H. Li, L. Sun, *Cem. Concr. Compos.*, 91 (2018) 21.
25. M. Chen, P. Gao, F. Geng, L. Zhang, H. Liu, *Constr. Build. Mater.*, 142 (2017) 320.
26. L.-J. Ouyang, W.-Y. Gao, B. Zhen, Z.-D. Lu, *Compos. Struct.*, 162 (2017) 294.
27. J. Hou, D. Chung, *Corros. Sci.*, 42 (2000) 1489.
28. P. Garcés, L.G. Andión, I. De la Varga, G. Catalá, E. Zornoza, *Corros. Sci.*, 49 (2007) 2557.
29. W. Li, S.C.M. Ho, D. Patil, G. Song, *Struct. Health Monit.*, 16 (2017) 674.
30. H. Qureshi, M. Saleem, *Materials*, 11 (2018) 2596.
31. Ö. Can, *Constr. Build. Mater.*, 186 (2018) 854.
32. X. Zheng, *Chem. Eng. Trans.*, 66 (2018) 1141.
33. Y. Li, X. Liu, M. Wu, W. Bai, *Constr. Build. Mater.*, 153 (2017) 436.
34. M. Mastali, A. Dalvand, A. Sattarifard, *Compos. Part B Eng.*, 112 (2017) 74.
35. J. Leppäniemi, P. Sippola, M. Broas, J. Aromaa, H. Lipsanen, J. Koskinen, *Thin Solid Films*, 627 (2017) 59.
36. R. Bonzom, R. Oltra, *Electrochem. Commun.*, 81 (2017) 84.
37. K.C. Mutyala, E. Ghanbari, G. Doll, *Thin Solid Films*, 636 (2017) 232.
38. L. Machuca Suarez, K. Lepkova, E. Suarez, *Corros. Mater.*, 44 (2019) 80.
39. J. Ji, D. Robert, C. Zhang, D. Zhang, J. Kodikara, *Struct. Saf.*, 64 (2017) 62.
40. R.B. Eckert, T.L. Skovhus, *Int. Biodeterior. Biodegrad.*, 126 (2018) 169.
41. J. Arellano-Pérez, O.R. Negrón, R. Escobar-Jiménez, J. Gómez-Aguilar, J. Uruchurtu-Chavarín, *Measurement*, 122 (2018) 73.
42. M.T. Alhaffar, S.A. Umoren, I.B. Obot, S.A. Ali, *RSC Adv.*, 8 (2018) 1764.
43. Y. Hayatgheib, B. Ramezanzadeh, P. Kardar, M. Mahdavian, *Corros. Sci.*, 133 (2018) 358.
44. A. Groysman, *Koroze Ochr. Mater.*, 61 (2017) 100.
45. F. Xu, Y. Chen, X. Zheng, R. Ma, H. Tian, *Materials*, 12 (2019) 753.
46. J. Fang, Z. Xie, G. Wallace, X. Wang, *Appl. Surf. Sci.*, 412 (2017) 131.
47. C. Yang, E. Trikantzopoulos, C.B. Jacobs, B.J. Venton, *Anal. Chim. Acta*, 965 (2017) 1.
48. J. Jiang, X. Yao, C. Xu, Y. Su, L. Zhou, C. Deng, *Compos. Part Appl. Sci. Manuf.*, 95 (2017) 248.
49. L. Teng, J. Weiliang, X. Chen, M. Jianghong, *J. Chin. Soc. Corros. Prot.*, 37 (2017) 382.
50. B. Li, W. Zhang, *Int J Electrochem Sci*, 12 (2017) 8432.

51. Y. Hoshi, C. Hasegawa, T. Okamoto, M. Soukura, H. Tokieda, I. Shitanda, M. Itagaki, Y. Kato, *Electrochemistry*, 87 (2019) 78.
52. R.B. Figueira, *Appl. Sci.*, 7 (2017) 1157.
53. Y. Bellal, S. Keraghel, F. Benghanem, T. Linda, G. Sığırcık, B. Riadh, A. Ourari, *Int J Electrochem Sci*, 13 (2018) 7218.
54. S. Li, B. Hu, F. Zhang, *J. Nanoelectron. Optoelectron.*, 12 (2017) 1244.
55. Y. Hoshi, T. Koike, H. Tokieda, I. Shitanda, M. Itagaki, Y. Kato, *J. Electrochem. Soc.*, 166 (2019) C3316.
56. W. Xu, J. Lu, W. Huo, J. Li, X. Wang, C. Zhang, X. Gu, C. Hu, *Nanoscale*, 10 (2018) 14304–14313.
57. P. Carrera, P.J. Espinoza-Montero, L. Fernández, H. Romero, J. Alvarado, *Talanta*, 166 (2017) 198.
58. Y. Zhang, J. Xiao, Y. Sun, L. Wang, X. Dong, J. Ren, W. He, F. Xiao, *Biosens. Bioelectron.*, 100 (2018) 453.
59. A. Adan-Mas, T.M. Silva, L. Guerlou-Demourgues, M.F. Montemor, *Electrochimica Acta*, 289 (2018) 47.
60. E.F. Pieretti, M. Neves, *Int. J. Electrochem. Sci.*, 12 (2017) 9204.
61. X. Meng, Z. Li, Z. Zhang, *Mater. Res. Bull.*, 99 (2018) 471.
62. Y. Liu, Z. Song, W. Wang, L. Jiang, Y. Zhang, M. Guo, F. Song, N. Xu, *J. Clean. Prod.*, 214 (2019) 298.
63. C. Chen, L. Jiang, M.-Z. Guo, P. Xu, L. Chen, J. Zha, *Constr. Build. Mater.*, 228 (2019) 116752.
64. Z. Zhang, F. Wang, Y. Liu, S. Wu, W. Li, W. Sun, D. Guo, J. Jiang, *RSC Adv.*, 8 (2018) 20648.
65. X. Feng, R. Shi, X. Lu, Y. Xu, X. Huang, D. Chen, *Corros. Sci.*, 124 (2017) 150.
66. D.-H. Xia, C. Ma, S. Song, L. Ma, J. Wang, Z. Gao, C. Zhong, W. Hu, *Sens. Actuators B Chem.*, 252 (2017) 353.
67. I. Obot, I.B. Onyeachu, *J. Mol. Liq.*, 249 (2018) 83.
68. M. Stefanoni, U.M. Angst, B. Elsener, *Sci. Rep.*, 8 (2018) 1.
69. M.A. Chidiebere, S. Nwanonenyi, D. Njoku, N.B. Iroha, E.E. Oguzie, Y. Li, *World News Nat. Sci.*, 15 (2017) 1.
70. L. Coelho, M. Taryba, M. Alves, M. Montemor, M.-G. Olivier, *Electrochimica Acta*, 277 (2018) 9.